Seeded QED cascades in counterpropagating laser pulses

T. Grismayer,[1,*] M. Vranic,[1] J. L. Martins,[1] R. A. Fonseca,[1,2] and L. O. Silva[1,†]
[1]*GoLP/Instituto de Plasmas e Fusão Nuclear, Universidade de Lisboa, Lisbon, Portugal*
[2]*DCTI/ISCTE Instituto Universitário de Lisboa, 1649-026 Lisboa, Portugal*
(Received 23 November 2015; revised manuscript received 17 December 2016; published 27 February 2017)

The growth rates of seeded QED cascades in counterpropagating lasers are calculated with first-principles two- and three-dimensional QED-PIC (particle-in-cell) simulations. The dependence of the growth rate on the laser polarization and intensity is compared with analytical models that support the findings of the simulations. The models provide insight regarding the qualitative trend of the cascade growth when the intensity of the laser field is varied. A discussion about the cascade's threshold is included, based on the analytical and numerical results. These results show that relativistic pair plasmas and efficient conversion from laser photons to γ rays can be observed with the typical intensities planned to operate on future ultraintense laser facilities such as ELI or Vulcan.

DOI: 10.1103/PhysRevE.95.023210

I. INTRODUCTION

The process of electron-positron pair creation from photon decay has been known since the early 1930s, but only the striking E-144 SLAC experiment [1,2] first demonstrated the possibility of producing matter directly via light-by-light scattering. The limits of the laser technology ($I \sim 10^{19}$ W/cm^2) at the time constrained the experiments to use the ultrarelativistic SLAC electron beam in order to reach the quantum electrodynamic (QED) regime necessary for the observation of pair production. The recent spectacular rise in laser intensities, accompanied by the ongoing construction of new laser facilities such as ELI [3] or the Vulcan 20 PW Project [4], will place intensities above 10^{23} W/cm^2 within reach, thus allowing for the exploration of new physics regimes [5]. Different laser configurations that have been envisaged to lower the intensity threshold [6] in order to observe Schwinger-like pair creation but prolific vacuum pair production require higher intensities than those mentioned earlier. Therefore, one ought to consider pair creation through the decay of high-energy photons in intense fields. This process usually leads to QED cascades, as the pairs created reemit hard photons that decay anew in pairs, eventually resulting in an electron-positron-photon plasma. QED cascades, also known as electronic or electromagnetic showers [7–10] when the external field is purely magnetic, have been studied theoretically in different electromagnetic configurations [11–14]. Notably, Bell and Kirk [15] suggested a judicious configuration comprising two circularly polarized counterpropagating lasers with some electrons in the interaction region to seed the cascade. They predicted prolific pair production for intensities approaching 10^{24} W/cm^2 for a μm wavelength laser. Recently, several groups [16–18] have pioneered the investigation of such cascades in a counterpropagating laser setup with particle-in-cell (PIC) simulations in which QED phenomena such as photon emission and pair creation have been added. In this paper, we intend to determine qualitatively the conditions under which driven cascades operate. We resort to two- and three-dimensional (2D and 3D) QED-PIC simulations to calculate their associated growth rates for different laser polarizations and for a wide range of intensities. The numerical results are then compared to an analytical model in two asymptotic limits. This model paves the way for determining the optimal conditions to generate dense electron-positron plasmas in the laboratory.

II. SIMULATIONS

Our exploration relies on a QED module, part of our PIC code OSIRIS 3.0 [19], which includes real photon emission from an electron or a positron, and the decay of photons into pairs, i.e., the Breit-Wheeler process. The differential probability rates describing these processes can be found in [10,20–23]. The implementation of such a module has already been described in detail elsewhere [16,24–28]. Many QED-PIC simulations have been performed in order to benchmark our module with previous results [16,17,24,26,29]. The exponential growth in the number of PIC particles, which is a critical numerical issue, is sorted out with the use of a novel particle-merging algorithm [30] that resamples the 6D phase space with different weighted macroparticles, allowing parameter scans in two and three dimensions. The algorithm preserves the total energy, momentum, and charge as well as the particle phase-space distribution, whereas previous attempts to merge particles were only focused on the conservation of some of the physical quantities [31–33].

To motivate our discussion, we first present simulations in which we have explored three configurations of colliding laser pulses whose polarization can either be linear or circular. The three-dimensional development of the cascade is shown in Fig. 1 for a different configuration. By examining the geometry of the standing waves, we can develop an intuitive picture of how the particles are accelerated, and hence we can predict which configuration will be optimal. For a given a_0, the optimal configuration consists in favoring the maximal pair growth and hence determining which field configuration offers on average the highest values of $\chi = (e\hbar/m^2c^3)\sqrt{(\gamma\vec{E} + \vec{u}\times\vec{B})^2 - (\vec{u}\cdot\vec{E})^2}$ with $\vec{u} = \vec{p}/mc$. It should be emphasized that radiation reaction in intense fields

*thomas.grismayer@ist.utl.pt
†luis.silva@ist.utl.pt

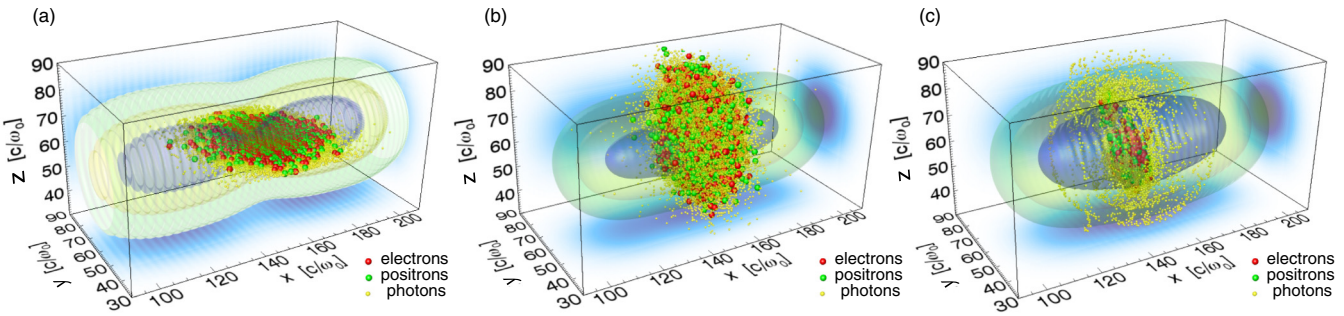

FIG. 1. 3D PIC simulation snapshot of QED cascades for (a) setup 1 with $a_0 = 1000$ at $t = 90\omega_0^{-1}$, (b) setup 2 with $a_0 = 1300$ at $t = 80\omega_0^{-1}$, and (c) setup 3 with $a_0 = 2000$ at $t = 46\omega_0^{-1}$. The laser pulses are shown through isocontours of the electromagnetic energy. The particles displayed represent only a small fraction of the simulation particles.

modifies the orbits of particles [34] and can lead to anomalous radiative trapping [35], which we omit in the following analysis but which is self-consistently captured in our simulations.

Setup 1 (lp-lp) consists of two linearly polarized lasers where the phase and polarization are defined by

$$\vec{a}_\pm = (0, a_0 \cos(\omega_0 t \pm k_0 x), 0), \tag{1}$$

where "−" and "+" denote, respectively, a wave propagating in the positive and in the negative x direction. $a_0 = eE_0/m\omega_0 c$ is the Lorentz-invariant parameter, related to the intensity I by $a_0 = 0.85(I[10^{18}\ \mathrm{W\,cm^{-2}}]\lambda_0^2\ [\mu\mathrm{m}])^{1/2}$, and E_0 is the peak electric field strength (which will be expressed is units of $m\omega_0 c/e$ in the following, such that $\tilde{E}_0 = eE_0/m\omega_0 c = a_0$). This results in a standing wave where $E_y = 2a_0 \cos(k_0 x)\sin(\omega_0 t)$ and $B_z = -2a_0 \sin(k_0 x)\cos(\omega_0 t)$; the electric and magnetic fields of the standing wave have a fixed direction. In addition, $\vec{E} \perp \vec{B}$ and there is a $\pi/2$ phase offset between $\vec{E}$ and $\vec{B}$ both in space and time. This suggests that the dynamics of the particles in the standing wave might be dominantly affected by the electric or the magnetic field depending on the phase within the temporal cycle [17,34]. The electric field accelerates electrons in the y direction, the magnetic field B_z can rotate the momentum vector and produce also p_x, and the orbits are confined in the x-y plane; see Fig. 1(a). The existence of the p_x component ensures that there is a perpendicular momentum component to both $\vec{E}$ and $\vec{B}$. Rotating the momentum vector toward higher p_x gradually increases χ_e until a photon is radiated. This photon then propagates and can decay far from the emission point. For a particle born at rest, χ_e oscillates approximatively twice per laser period with a maximum on the order of $2a_0^2/a_S$, where $a_S = mc^2/\hbar\omega_0$ is the normalized Schwinger field [36]. The cascade develops mostly around the bunching locations (two per wavelength, which corresponds to the moment of rotation or high χ) and is characterized by a growth rate that possesses an oscillating component at $2\omega_0$.

Setup 2 (cw-cw) is composed of two clockwise circularly polarized lasers defined by

$$\vec{a}_\pm = (0, a_0 \cos(\omega_0 t \pm k_0 x), \pm a_0 \sin(\omega_0 t \pm k_0 x)), \tag{2}$$

where $a_0 = 0.6(I[10^{18}\ \mathrm{W\,cm^{-2}}]\lambda_0^2\ [\mu\mathrm{m}])^{1/2}$. In addition to the E_y and B_z components that are the same as for the lp-lp case, we also have $E_z = 2a_0 \sin(k_0 x)\sin(\omega_0 t)$ and $B_y = -2a_0 \cos(k_0 x)\cos(\omega_0 t)$. For any x, both $\vec{E}$ and $\vec{B}$ are parallel to the vector $\vec{e}(x) = (0, \cos x, \sin x)$. The direction of the fields depends on the position, but the amplitude of both $\vec{E}$ and $\vec{B}$ is only a function of time, which results in a helical field structure growing or shrinking uniformly in space ($\vec{E}$ and $\vec{B}$ are dephased by $\pi/2$ in space). Contrary to the lp-lp setup, this configuration does not produce p_x for particles born at rest since at each position both $\vec{E}$ and $\vec{B}$ are parallel to the momentum at all times, and significant χ_e cannot be achieved. Reaching high values of χ_e is, however, possible for particles that are not at rest initially. If an external perturbation provides a transverse momentum p_x (e.g., the initial ponderomotive force due to the laser pulse envelope), the particle can move along the x axis and leave the region where the fields remain parallel to the momentum kick acquired at the initial position. In this way, the value of χ_e is increased, and so is the probability of radiating hard photons. The decay of hard photons produces pairs that will possess either an initial transverse or longitudinal momentum component, and the cascade will naturally develop. A crude analysis shows that the maximal χ_e attainable is on the order of $2a_0\gamma_0/a_S$ (γ_0 being the initial energy of the particle when created). All x positions have equivalent probabilities to initiate a cascade because only the azimuthal angle of the field changes along the x axis. Therefore, the cascade shall develop over the entire wavelength.

Setup 3 (cw-cp) is formed by a clockwise and a counterclockwise polarized laser:

$$\vec{a}_\pm = (0, a_0 \cos(\omega_0 t \pm k_0 x), -a_0 \sin(\omega_0 t \pm k_0 x)), \tag{3}$$

where $a_0 = 0.6(I[10^{18}\ \mathrm{W\,cm^{-2}}]\lambda_0^2\ [\mu\mathrm{m}])^{1/2}$. The components E_y and B_z are the same, but $E_z = 2a_0 \cos(k_0 x)\cos(\omega_0 t)$ and $B_y = -2a_0 \sin(k_0 x)\sin(\omega_0 t)$. The magnitude of the field vectors is constant in time ($|\vec{E}| = 2a_0 \cos x$ and $|\vec{B}| = 2a_0 \sin x$), whereas the direction changes. In this case, $\vec{E} \| \vec{B}$, and their direction $\vec{e}(t) = (0, \cos t, \sin t)$ does not depend on space, which results in a fixed planar beating pattern that rotates around the laser propagation axis. This setup consists in a rotating field structure, and the dynamics of the particles has already been studied [15,26,37]. The advantage lies in the direction of the fields, which is constantly changing, and the particles are not required to move in x to enter a region where $\vec{E}$ and $\vec{B}$ are perpendicular to their momentum. For similar $p_\perp$, the χ_e is on the same order regardless of the x position, so we could expect the cascade to grow everywhere with the same

probability. However, the particle acceleration is stronger in the regions of high electric field, so the highest electron momenta are obtained where the electric field is maximum. This then leads to higher χ_e, and the cascade develops favorably in the region of strong electric field (precisely in the node where $B = 0$ [15]), producing a plasma wheel as shown in Fig. 1(c). At this particular position, the parameter χ_e can reach a maximal value of $2a_0^2/a_S$ [26].

From the description of the three configurations, it seems clear that the second setup can be considered nonoptimal in view of the low values of χ_e. Rigorously, setup 1 can produce the highest values of χ_e ($\chi_e > 2a_0^2/a_S$) but only for particles born in a specific phase of the standing wave. The majority of the particles are sloshing back and forth between the electric and magnetic zone, which results in lower average χ_e in comparison with setup 3. The efficiency of the cascade setups can be more accurately assessed by computing its growth rate Γ. We measure the growth rate in simulations, and we compare it to the analytical prediction when possible. As a matter of fact, a full analytical treatment is not always possible due to the complexity of the stochastic orbits in the standing wave. We introduce here models that allow us to retrieve the asymptotic limit of the growth rate.

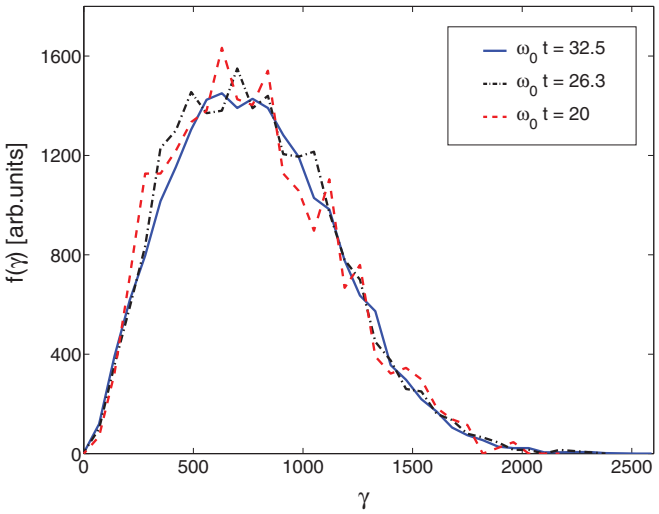

FIG. 2. Electron energy distribution function at different times for $a_0 = 500$ in the case of a pure uniform rotating field. The energy distribution is shown at three different times: red solid line at $\omega_0 t = 20$, black dash-dotted line at $\omega_0 t = 26.3$, and blue dashed line at $\omega_0 t = 32.5$.

III. CASCADE MODELS

A. Ideal model

For a collection of identical photons n_γ, whose probability rate to decay into a pair is given by W_p, the number of pairs created after a time t is $n_p = n_\gamma(1 - e^{-W_p t})$. If the photons originate from a source that emits constantly at a rate W_γ, we get $n_p = \int_0^t dt' W_\gamma (1 - e^{-W_p(t-t')})$. The rate of created pairs is then

$$\frac{dn_p}{dt} = \int_0^t dt' W_\gamma W_p e^{-W_p(t-t')}. \tag{4}$$

If the source of the emitted photons is the pairs, the number of photons created during a time dt', being $2dt' W_\gamma$, has to be multiplied by the current number of pairs, $n_p(t')$. The rate of pairs is now

$$\frac{dn_p}{dt} = 2\int_0^t dt' n_p(t') W_\gamma W_p e^{-W_p(t-t')}. \tag{5}$$

This equation can be solved using the Laplace transform. Defining the Laplace variable as s, Eq. (5) becomes

$$\hat{n}(s) = \frac{n(0)}{s - \frac{2W_\gamma W_p}{s+W_p}}. \tag{6}$$

The behavior of n_p, defined as the inverse Laplace transform of $\hat{n}$, depends at late times, $t \gg W_\gamma^{-1}, W_p^{-1}$, on the contribution of the singularities of $\hat{n}$. These singularities are the roots of the polynomial $s^2 + W_p s - 2W_\gamma W_p = 0$ that admits a positive and a negative solution,

$$s_\pm = \frac{W_p}{2}\left(-1 \pm \sqrt{1 + 8\frac{W_\gamma}{W_p}}\right), \tag{7}$$

where the positive solution s_+ is consistent with the result derived by Bashmakov [17]. A pole at $s_\pm$ gives a contribution scaling as $e^{s_\pm t}$, thus the function $n_p(t)$ grows exponentially with a growth rate $\Gamma = s_+$. It is interesting to look at how the growth rate depends on the characteristic rate as the ratio $r = W_\gamma / W_p$ between them evolves,

$$\Gamma \simeq \begin{cases} 2W_\gamma & \text{if } r \ll 1, \\ W_p \sim W_\gamma & \text{if } r \sim 1, \\ \sqrt{2W_\gamma W_p} & \text{if } r \gg 1. \end{cases} \tag{8}$$

B. Rotating-field model

The case of a uniform rotating electric field constitutes a good approximation of the standing-wave field produced in setup 3 [15]. The advantage of this setup is that the cascade develops mostly in one spot, $x = 0$, which allows us to assume a time-dependent field. In a fully self-consistent kinetic model, we would have to follow all particles including the quantum radiation reaction for their stochastic orbits, which appears to be overly cumbersome. Since the growth of the cascading process in a uniform rotating electric field is purely exponential [26], this means somehow that the electron (or positron) energy distribution remains almost constant during the development of the cascade (the number of particles increases but the shape of the distribution is not altered). This implies that in the tail of the distribution, the high-energy particles, which lose energy-emitting photons, are constantly replaced by newly created particles being reaccelerated. Figure 2 shows the electron energy distribution at three different times (the details of the simulation parameters are thoroughly discussed in Sec. IV). These three times are taken at consecutive rotation periods of the electric field, and one can notice that the shape of the distribution remains constant as the number of pairs grows in the system. We can then suppose that the pairs follow a fluidlike behavior that can be described through an average energy $\bar{\gamma}$ and an average quantum parameter $\bar{\chi}_e$. We generalize

Eq. (5) in the following form:

$$\frac{dn_p}{dt} = 2\int_0^t dt' \int d\chi_\gamma n_p(t') \frac{d^2P}{dt'd\chi_\gamma} W_p e^{-W_p(t-t')}. \quad (9)$$

The differential probability rate $d^2P/dt'd\chi_\gamma$ depends thus on $\bar{\gamma}$, $\bar{\chi}_e$, and χ_γ. We further assume that the photon decay rate (or the pair emission probability rate) can be considered as constant in time, which permits us to write $W_p = W_p(\chi_\gamma, \epsilon_\gamma)$ with $\epsilon_\gamma = \bar{\gamma}\chi_\gamma/\bar{\chi}_e$. Equation (9) is solved in the same way as before for Eq. (5), and calculating Γ amounts to solving the zeros of

$$s - 2\int_0^{\bar{\chi}_e} d\chi_\gamma \frac{\frac{d^2P}{dt'd\chi_\gamma} W_p}{s + W_p} = 0. \quad (10)$$

1. Weak-field limit

When $\bar{\chi}_e \ll 1$, the pair creation probability can be approximated by [10,23] $W_p \simeq (3\pi/50)(\alpha/\tau_c)e^{-8/3\chi_\gamma}\chi_\gamma/\epsilon_\gamma$ and $d^2P/dt\,d\chi_\gamma \simeq \sqrt{2/3\pi}(\alpha/\tau_c)e^{-\delta}/(\delta^{1/2}\bar{\chi}_e\bar{\gamma})$ with $\delta = 2\chi_\gamma/[3\bar{\chi}_e(\bar{\chi}_e - \chi_\gamma)]$, $\tau_c = \hbar/mc^2$, and $\alpha = e^2/\hbar c$. We start from an assumption (which is verified by the result) that in the limit $\bar{\chi}_e \ll 1$, $W_p(\chi_\gamma) \ll s$, hence the zeros of s corresponding to a growing exponential ($\Gamma = s^+$) are given by

$$\Gamma \simeq \left(2\int_0^{\bar{\chi}_e} d\chi_\gamma \frac{d^2P}{dt\,d\chi_\gamma} W_p\right)^{1/2}. \quad (11)$$

This integrand in Eq. (11) is comprised of an exponential function multiplied by another function. More specifically, the argument of the exponential possesses a unique maximum, $\chi_{\gamma,0} = 2\bar{\chi}_e/3$, at which the second derivative of the argument is negative. One can thus evaluate the integral using Laplace's method: $\int h(x)e^{f(x)}dx \simeq \sqrt{2\pi/|f''(x_0)|}h(x_0)e^{f(x_0)}$, where x_0 is the unique maximum. In this case, $f(\chi_\gamma) = -\delta - 8/3\chi_\gamma$, $f(\chi_{\gamma,0}) = -16/3\bar{\chi}_e$, $f''(\chi_{\gamma,0}) = -54/\bar{\chi}_e^3$, and $h(x_0) = 1/\sqrt{\delta(\chi_{\gamma,0})} = \sqrt{3\bar{\chi}_e}/2$. We obtain for the growth rate in the weak-field limit

$$\Gamma \simeq \frac{1}{5}\sqrt{\frac{\pi}{6^{1/2}}}\frac{\alpha}{\tau_c}\frac{\bar{\chi}_e e^{-8/3\bar{\chi}_e}}{\bar{\gamma}}. \quad (12)$$

The last step consists in finding how $\bar{\gamma}$ and $\bar{\chi}_e$ depend on a_0. In a rotating field mocking the beating of two 1 μm lasers [12,15,26], $\vec{a} = a_r[\cos(\omega_0 t), \sin(\omega_0 t)]$ ($a_r = 2a_0$), it is clear from Eq. (11) that $\Gamma \ll \omega_0$ for $\bar{\chi}_e \ll 1$. Thus $\bar{\gamma}$ and $\bar{\chi}_e$ can be approximated by their average values over a laser cycle. The expressions of $\gamma(t)$ and $\chi_e(t)$ can be found in [26], and for $a_r \gg 1$ (neglecting the quantum recoil) one finds $\bar{\gamma} \simeq \langle\gamma\rangle = 4a_r/\pi$ and $\bar{\chi}_e \simeq \langle\chi_e\rangle = a_r^2/a_S$. Although not shown in this article, these estimates are close to the average energy and the average quantum parameter of the particles in the simulations.

2. Strong-field limit

When $\bar{\chi}_e \gg 1$, W_γ and W_p have similar asymptotic expressions, and Fedotov [37] obtained with intuitive considerations an estimate for the growth rate $\Gamma \sim W_p \sim W_\gamma(\bar{\chi}_e, \bar{\gamma})$. While it is not an exact solution, one can verify that this result is somehow consistent with Eq. (10). In this limit, where the recoil cannot be omitted, $\Gamma \gg \omega_0$ and the values of $\bar{\gamma}$ and $\bar{\chi}_e$ can be evaluated as [37] $\bar{\gamma} \sim \gamma(t = W_\gamma^{-1}) \simeq \mu^{3/4}\sqrt{a_S}$ and $\bar{\chi}_e \sim \chi_e(t = W_\gamma^{-1}) \simeq 1.24\mu^{3/2}$ with $\mu = a_r/(\alpha a_S)$. Taking the characteristic energy for photon emission at the moment W_γ^{-1} has been proven to be a valuable and accurate prediction [26]. Unfortunately, it is not possible to obtain a simple analytical expression for the growth rate in such a limit, and we resorted to a numerical computation of Eq. (10).

These two asymptotic limits are a generalization of the growth rate obtained in the ideal model for $r \sim 1$ and $r \gg 1$. The case $r \ll 1$ is not physically relevant since photon emission is always more probable than pair emission.

IV. PHYSICAL SETUP AND LASER PARAMETERS

The laser parameters we chose are based on the typical parameters expected in future laser facilities such as Vulcan or ELI [3,4,38], a 10 PW peak-power system, 100 J–1 kJ, 30–60 fs, and a focal spot that could be as small as a micron. We have also pushed the parameters in order to make the bridge between different regimes: the onset of QED characterized by $\chi \ll 1$ [12,15,28] and the full QED-dominated regime for $\chi \gg 1$, which have been explored in prior studies [16,17,26,37].

One of the objectives of these future facilities is indeed to focus these ultraintense lasers to a micron spot size, and this can probably be achieved by using adequate optics. Nonetheless, from a theoretical point of view, focusing a laser pulse to a given waist requires knowing the self-consistent shape of the pulse far away from the focus point. The seminal article on electromagnetic beams from Davis [39] shows how to construct light paraxial beams whose formal solution employs an expansion in power of W_0/z_r, where W_0 is the beam waist and z_r is the diffraction length. The well-known solution used in the literature for Gaussian beams requires $W_0 \ll z_r$ or equivalently $\lambda_0 \ll W_0$ (λ_0 being the central wavelength of the laser beam). Hence, a paraxial beam is not an accurate solution for a beam that is aimed at $\lambda_0 \simeq W_0$. Furthermore, it has also been proven [40] that focusing a laser beam to the diffraction limit requires inclusion of terms of fifth order in the diffraction parameter W_0/z_r in the description of the associated fields. Another conclusion drawn from this latter article is that the electron dynamics in a tightly focused beam is not adequately described by the plane-wave approximation because of the extra components of the field, which must be considered to satisfy $\vec{\nabla}\cdot\vec{E} = 0$ and $\vec{\nabla}\cdot\vec{B} = 0$ in vacuum.

In our simulations, all the laser pulses have a $\lambda_0 = 1$ μm central wavelength and the same spatiotemporal envelope functions, with differences in the fast-oscillating components that will be presented separately for different polarizations. The envelope function is transversally a Gaussian with a focal spot of 3.2 μm, while the temporal profile is given by $10\tau^3 - 15\tau^4 + 6\tau^5$, $\tau = t/\tau_0$ for $t \leqslant \tau_0$, and $\tau = 2\tau_0 - t$ for $\tau_0 < t \leqslant 2\tau_0$, where $\tau_0 = 32$ fs is the pulse duration at full width at half-maximum in the fields. The focal spot of 3.2 λ represents a compromise where we can ensure that the laser intensity at the focus is the one wanted and that in the region of the focus the structure of the fields is close to a plane wave. In OSIRIS, laser pulses are initialized far from the focus point where the transverse fields are given by the paraxial theory [39], whereas the longitudinal component is self-consistently computed using $\vec{\nabla}\cdot\vec{E} = 0$ and $\vec{\nabla}\cdot\vec{B} = 0$.

The laser pulses are initialized 20 μm away from one another. The focal plane for both lasers is located at half-distance between their envelope centers. A total of 100 test electrons are placed in the focal plane to seed the cascade in three dimensions (there are 10 electrons in each transverse direction, and they occupy an area of 1 c^2/ω_0^2). Two-dimensional simulations were seeded with 100 electrons in the transverse direction over a length of c/ω_0. We have also tested the seeding with one electron for 2D and 3D simulations where the electron was located at the very center of the focal plane. The simulation box is composed of 3000×1200 cells and $3000 \times 1200 \times 1200$ cells for two and three dimensions, respectively. The spatial resolution is $dx = dy = dz = 0.1c/\omega_0$, and after extensive convergence tests we have chosen $dt = 0.001\omega_0^{-1}$ ($\omega_0 = k_0 c = 2\pi c/\lambda_0$).

To put the model presented in the previous section to the test, we have also conducted a series of simulations with a uniform rotating electric field. The rotating field is imposed as an external field and is turned on during the duration of the simulation, and it has the following structure: $E_x = a_0 \cos(\omega_0 t)$ and $E_y = a_0 \sin(\omega_0 t)$. The spatial uniformity of the electric field allows us to use a small simulation box with periodic boundary conditions. Nonetheless, the time resolution is still conditioned by the pair and photon characteristic emission time, and we have thus kept $dt = 0.001\omega_0^{-1}$.

V. DISCUSSION AND CONCLUSION

As was shown recently by Jirka *et al.* [18], the spatial structure of cascading plasma is essential to understanding where the pairs are produced. Additionally, the growth rate of the cascade is the important macroscopic quantity that tells how the number of pairs rises in the interaction region. As a matter of fact, as we will see in this section, the growth rate of the cascade depends on the polarization of the lasers that produce different field structures. Additionally, the growth rate of the cascade can only be determined in an unambiguous manner when the density of the pair plasma is relativistically underdense such that the self-generated field remains negligible compared to the external fields provided by the overlap of the two lasers. The case of relativistically overdense pair plasmas is of high relevance for laser absorption, and this problem has been addressed with QED-PIC showing that significant absorption can be achieved for $I > 10^{24}$ W/cm^2 and pulses of a few 10's of fs as first demonstrated by Nerush [16] and later by Grismayer [41]. As mentioned previously, the focal spot of both lasers is 3.2 microns, which is still in the paraxial approximation for a one-micron wavelength and thus ensures that at the focus, the field structure of the laser can be described by a plane wave. We have actually performed several simulations with pure plane standing waves and compared the growth rate of the cascade with situations where realistic pulses were used without significant differences, as can be seen in Table I. It should be stressed that we measure the growth rate in a realistic setup when the two lasers are around the point of full overlap in order to make sensible comparisons with ideal setups (such as the uniform rotating field).

Figure 3 shows the growth rate for different configurations as a function of a_0. The simulation results for the pure rotating electric field configuration are displayed with black squares and lines. The growth rate given by Eq. (11) and the numerical solution of Eq. (10) depicted by the blue and green dashed lines, respectively, are in good agreement with the rotating-field simulation results in the limit of their validity ($a_0 \ll$

TABLE I. Growth rate for the plane wave and for laser pulses. The growth rate is measured in units of the plane-wave or laser pulse frequency ω_0. PW stands for plane wave, whereas pulse stands for the simulation performed with realistic laser pulses whose parameters are described in the text.

a_0	1000	1500	3000	5000
type	pulse/PW	pulse / PW	pulse/PW	pulse/PW
$\Gamma_{\text{cw-cp}}$	0.85/0.82	1.35/1.39	2.4/2.39	3.35/3.38
$\Gamma_{\text{lp-lp}}$	0.28/0.25	0.56/0.52	0.85/0.82	1.2/1.05
$\Gamma_{\text{cw-cw}}$	0.13/0.14	0.17/0.15	0.2/0.19	0.25/0.23

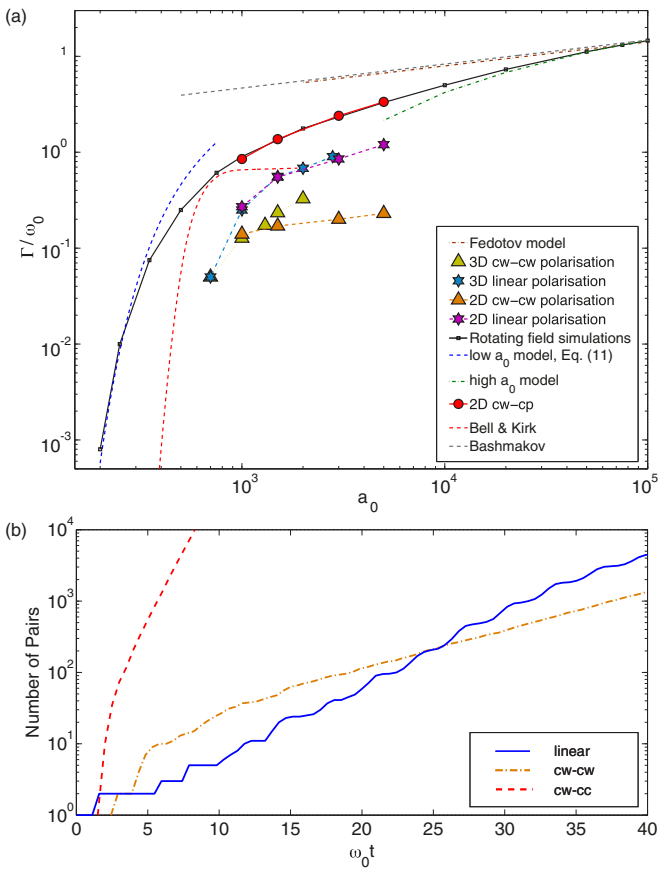

FIG. 3. (a) Growth rate as a function of a_0 for different laser polarization. The low a_0 model, depicted by a dashed blue (dark gray) line, corresponds to Eq. (11), and the high a_0 model, depicted by a dash-dotted green (light gray) line, corresponds to the numerically integrated Eq. (10) with $\bar{\gamma} = \mu^{3/4}\sqrt{a_S}$ and $\bar{\chi}_e = 1.24\mu^{3/2}$. The model of Bell and Kirl is shown by a dashed red (light gray) dashed line, the model of Bashmakov is shown by a gray (upper) line, and the model of Fedotov is displayed by a dash-dotted brown (light gray) line. (b) Onset of QED cascades for the three setups for $a_0 = 1000$; the linear polarization setup is shown by the solid blue (dark gray) line, the cw-cw setup by the dash-dotted orange (light gray) line, and the cw-cc setup by the dashed red (dark gray) line.

10^3 for $\bar{\chi}_e \ll 1$ and $a_0 \gg 10^3$ for $\bar{\chi}_e \gg 1$). As expected, the growth rates in the cw-cc setup match those of the rotating-field configuration. This growth rate is the highest of all three configurations for a fixed a_0. To underscore the improvement of our model compared to previous ones, we have also plotted the growth rate derived by Bell and Kirk [15] with a red dashed line, the rate derived by Bashmakov [17] with a gray dashed line and the result given by Fedotov [37] with a dash-dotted brown line. In the weak-field regime, the rate coming from the model of Bell and Kirk is low in comparison with our analytical and numerical study. Even though their model and ours are essentially the same, one of the reasons for the mismatch is that the successive approximations made by Bell and Kirk led to an underestimate of the photon optical depth. In the strong field regime, both prior models [17,37], which possess the same scaling, appear to be valuable predictions for extreme intensities ($a_0 \gg 10^4$). The small discrepancy, which occurs at lower intensity, with our analytical results (green dashed curve) results from the approximation $\Gamma \sim W_p \sim W_\gamma$. As discussed before, while this ordering is appropriate, numerical factors (which are neglected) are sufficient to cause a departure from the numerical results.

The lp-lp setup has a growth rate lower than the cw-cc configuration, but higher than the cw-cw configuration. Figure 3(b) also confirms the $2\omega_0$ oscillating component of the lp-lp growth rate. There is no appreciable difference in the growth rate of the 2D and 3D simulations for linearly polarized lasers. The lowest growth rate is attributed to the cw-cw configuration, and this is also in agreement with our previous analysis. Finite-size Gaussian laser pulses can provide an initial nonzero p_x in order to seed the cascade. The gradients of the intensity that provide the ponderomotive force are more pronounced in three dimensions (they affect a higher percentage of the particles), and therefore the growth rate in this configuration becomes slightly higher in 3D simulations than in 2D simulations. This configuration is robust because there are no special favorable locations for the cascade seeding. On the contrary, the seeding with electrons of the cw-cc setup turns out to be difficult. The reason is that efficient growth happens only in the regions around the maximum of the electric field. By starting a cascade with only a few electrons, it is not guaranteed that they will enter such a region. This is precisely why there are no 3D data for the cw-cc configuration in Fig. 3(a): the cascade has not started below $a_0 = 2000$ even though the same initial conditions were used as in setups 1 and 2. Similar conclusions have been drawn by Jirka [18], who recommends the linear polarization setup in order to maximize the number of pairs created.

A crucial question addressed by Fedotov *et al.* [37] concerns the cascade threshold, which according to the latter author is around $I_{\text{th}} > 2.5 \times 10^{25}$ W/cm^2 or $a_r > \alpha a_S$. Fundamentally speaking, there is no threshold for the cascading process since the growth rate never vanishes (even though it is reduced exponentially for lower a_0's). Notwithstanding, a very low growth rate requires a very long laser duration as well as a gigantic spot size in order to show evidence of the cascade. A convincing definition of the threshold can therefore be the minimum growth rate required to observe a significant amount of pairs produced, i.e., few e-folding of the cascade, $\Gamma\tau_c \gtrsim 1$, where τ_c is the characteristic time during which the process occurs. Fedotov *et al.* [37], who established a valid model in the strong-field limit, identified two characteristic times: the acceleration time, which is the time required to reach $\chi \simeq 1$, and the escaping time, which is the duration of a particle (pairs or photon) in the laser pulse. The minimum growth rate lies probably in the the weak-field limit where $\chi < 1$, so the acceleration time is not necessary. However, the escaping time is still relevant in our case and can be generalized as $t_{\text{esc}} \sim W_0/c$. Using Eq. (11), we obtain a new threshold given by

$$a_0 > \sqrt{\frac{2a_S}{3\log\left(\frac{\pi a_0 \alpha W_0 c}{8\omega_0}\right)}}. \tag{13}$$

For $W_0 = 3.2\ \mu$m, $a_0 > 310$ or $I > 2.7 \times 10^{23}$ W/cm^2, which is two orders of magnitude lower than the threshold derived initially by Fedotov *et al.* [37]. One should notice that in a recent publication [42], the same author recognized that the initial criteria, $a_r > \alpha a_S$, in fact overestimate the actual cascade threshold for three main reasons: (i) simulations show cascade development at a lower intensity, (ii) the escaping time may be larger, and (iii) pairs can only be created when $\chi_\gamma \gtrsim 1$.

We shall now consider what the threshold is for the cascading process, taking into account the laser parameters of future facilities. The laser power should theoretically rise up to 10 PW. For a focal spot close to the diffraction limit, $W_0 \simeq \lambda_0$, the intensity could then reach $I \simeq 10^{24}$ W/cm^2. Applying the same criteria for the threshold, $\Gamma > 1/t_{\text{esc}}$, and using the results of Fig. 3(a), we find that in the case of the cw-cc setup, $a_0 > 400$, while for the lp-lp setup, $a_0 > 800$, which corresponds in both cases to intensities lower than $I = 10^{24}$ W/cm^2. We would like to warn the reader that these numbers are conjectural since we have not performed simulations for focal spots close to the diffraction limit. In addition, the injection of particles into the laser focus depends on several parameters, such as pulse focusing, pulse duration, as well as the initial position of the target, its size, shape, and composition (solid, gaseous) [43]. Therefore, information on the laser intensity alone may not be sufficient to fully characterize the cascade threshold and to guarantee that the cascade will take off. Nonetheless, our conjectural numbers appear to be on the same order as the threshold, $I_{\text{th}} = 1.7 \times 10^{24}$ W/cm^2, given by Gelfer [14], who used colliding laser beams with a central wavelength of $\lambda = 1.24\ \mu$m ($\hbar\omega = 1$ eV), a beam waist of $W = 2\sqrt{2}/\pi\lambda \simeq 0.9\lambda$ (which corresponds to tightly focused beams), and a pulse duration of 20 fs. If the focal spot was taken to be larger, such as the one we chose in this work, $W_0 = 3.2\ \mu$m, for linearly polarized lasers (which are the more likely to be delivered), observing a cascade will require $a_0 > 700$ or $I_{\text{th}} > 6.8 \times 10^{23}$ W/cm^2. This threshold can be verified in Table II for the laser pulse parameters considered in this study. The criterion for the threshold is $\Gamma W_0/c > 1$, which implies that every single electron contributing to the cascade will produce at least three new electrons during the interaction of the two laser pulses. This intensity corresponds to a peak power of $P = \pi W_0^2 I_{\text{th}}/2 \simeq 100$ PW.

In summary, the efficiency of QED cascades has been studied for three different laser intensities and configurations in 2D and 3D simulations. Whereas setup 3 seems to be promising

TABLE II. Number of pairs per initial electron obtained for linearly polarized laser pulses with $W_0 = 3.2\ \mu$m.

a_0	Dimension	Seeding	Pairs/e^-	Cascade
400	2D	100 electrons	0.01	✗
500	3D	100 electrons	0.03	✗
700	2D	100 electrons	10	✓
700	3D	one electron	30	✓

due to an unquestionably higher growth rate for a fixed a_0, the seeding of this latter configuration proves to be problematic. Setups 1 and 2 are more preferable to ensure the takeoff of the cascade. Using the growth rates of Fig. 3(a), we predict that the cascading process should start around $I > 7 \times 10^{23}$ W/cm^2 for a focal spot above the diffraction limit and 30 fs lasers. With an electron seeding composed of a micron-sized cryogenic hydrogen target, a relativistic critical density pair plasma $n_{\rm rc}$ can be created for the parameters expected for ELI [38] ($I > 10^{24}$ W/cm^2 for pulses of a few 10's of fs). Once the plasma reaches the density $n_{\rm rc}$, the laser starts to be efficiently converted into γ rays, and one approaches the condition to create a laboratory γ-ray pulsar [16,41,44]. This will be explored in future publications.

ACKNOWLEDGMENTS

This work is supported by the European Research Council (ERC-2015-AdG Grant No. 695088) and FCT (Portugal) Grants No. SFRH/BD/62137/2009 and No. SFRH/IF/01780/2013. We acknowledge PRACE for awarding access to resource SuperMUC based in Germany at Leibniz Research Center. Simulations were performed at the Accelerates cluster (Lisbon, Portugal), and SuperMUC (Germany).

[1] D. L. Burke, R. C. Field, G. Horton-Smith, J. E. Spencer, D. Walz, S. C. Berridge, W. M. Bugg, K. Shmakov, A. W. Weidemann, C. Bula, K. T. McDonald, E. J. Prebys, C. Bamber, S. J. Boege, T. Koffas, T. Kotseroglou, A. C. Melissinos, D. D. Meyerhofer, D. A. Reis, and W. Ragg, Phys. Rev. Lett. **79**, 1626 (1997).

[2] C. Bamber, S. J. Boege, T. Koffas, T. Kotseroglou, A. C. Melissinos, D. D. Meyerhofer, D. A. Reis, W. Ragg, C. Bula, K. T. McDonald, E. J. Prebys, D. L. Burke, R. C. Field, G. Horton-Smith, J. E. Spencer, D. Walz, S. C. Berridge, W. M. Bugg, K. Shmakov, and A. W. Weidemann, Phys. Rev. D **60**, 092004 (1999).

[3] Extreme light infrastructure, http://www.eli-laser.eu/

[4] The vulcan 10 petawatt project, http://www.clf.stfc.ac.uk/CLF/Facilities/Vulcan/The+Vulcan+10+Petawatt+Project/14684.aspx

[5] A. Di Piazza, C. Müller, K. Z. Hatsagortsyan, and C. H. Keitel, Rev. Mod. Phys. **84**, 1177 (2012).

[6] S. Bulanov, N. Narozhny, V. Mur, and V. Popov, J. Exp. Theor. Phys. **102**, 9 (2006).

[7] L. Landau and G. Rumer, Proc. R. Soc. London, Ser. A **166**, 213 (1937).

[8] A. I. Akhiezer, N. P. Merenkov, and A. P. Rekalo, J. Phys. G **20**, 1499 (1994).

[9] V. Anguelov and H. Vankov, J. Phys. G **25**, 1755 (1999).

[10] T. Erber, Rev. Mod. Phys. **38**, 626 (1966).

[11] S. S. Bulanov, T. Z. Esirkepov, A. G. R. Thomas, J. K. Koga, and S. V. Bulanov, Phys. Rev. Lett. **105**, 220407 (2010).

[12] J. G. Kirk, A. R. Bell, and I. Arka, Plasma Phys. Control. Fusion **51**, 085008 (2009).

[13] S. S. Bulanov, C. B. Schroeder, E. Esarey, and W. P. Leemans, Phys. Rev. A **87**, 062110 (2013).

[14] E. G. Gelfer, A. A. Mironov, A. M. Fedotov, V. F. Bashmakov, E. N. Nerush, I. Y. Kostyukov, and N. B. Narozhny, Phys. Rev. A **92**, 022113 (2015).

[15] A. R. Bell and J. G. Kirk, Phys. Rev. Lett. **101**, 200403 (2008).

[16] E. N. Nerush, I. Y. Kostyukov, A. M. Fedotov, N. B. Narozhny, N. V. Elkina, and H. Ruhl, Phys. Rev. Lett. **106**, 035001 (2011).

[17] V. F. Bashmakov, E. N. Nerush, I. Y. Kostyukov, A. M. Fedotov, and N. B. Narozhny, Phys. Plasmas **21**, 013105 (2014).

[18] M. Jirka, O. Klimo, S. V. Bulanov, T. Z. Esirkepov, E. Gelfer, S. S. Bulanov, S. Weber, and G. Korn, Phys. Rev. E **93**, 023207 (2016).

[19] R. A. Fonseca, L. O. Silva, F. S. Tsung, V. K. Decyk, W. Lu, C. Ren, W. B. Mori, S. Deng, S. Lee, T. Katsouleas, and J. C. Adam, *Lecture Notes in Computer Science* (Springer, Berlin, 2002), Vol. 2331, pp. 342–351.

[20] A. I. Nikishov and V. I. Ritus, Sov. Phys. JETP **25**, 1135 (1967).

[21] V. Baier and V. Katkov, Phys. Lett. A **25**, 492 (1967).

[22] N. P. Klepikov, Zh. Eksp. Teor. Fiz. **26**, 19 (1954).

[23] V. Ritus, J. Sov. Laser Res. **6**, 497 (1985).

[24] M. Lobet, E. d'Humieres, M. Grech, C. Ruyer, X. Davoine, and L. Gremillet, arXiv:1311.1107.

[25] T. G. Blackburn, C. P. Ridgers, J. G. Kirk, and A. R. Bell, Phys. Rev. Lett. **112**, 015001 (2014).

[26] N. V. Elkina, A. M. Fedotov, I. Y. Kostyukov, M. V. Legkov, N. B. Narozhny, E. N. Nerush, and H. Ruhl, Phys. Rev. ST Accel. Beams **14**, 054401 (2011).

[27] C. P. Ridgers, C. S. Brady, R. Duclous, J. G. Kirk, K. Bennett, T. D. Arber, A. P. L. Robinson, and A. R. Bell, Phys. Rev. Lett. **108**, 165006 (2012).

[28] R. Duclous, J. G. Kirk, and A. R. Bell, Plasma Phys. Control. Fusion **53**, 015009 (2011).

[29] S. Tang, M. A. Bake, H.-Y. Wang, and B.-S. Xie, Phys. Rev. A **89**, 022105 (2014).

[30] M. Vranic, T. Grismayer, J. Martins, R. Fonseca, and L. Silva, Comput. Phys. Commun. **191**, 65 (2015).

[31] A. N. Timokhin, Mon. Not. R. Astron. Soc. **408**, 2092 (2010).

[32] G. Lapenta, J. Comput. Phys. **181**, 317 (2002).

[33] G. Lapenta and J. U. Brackbill, J. Comput. Phys. **115**, 213 (1994).

[34] T. Esirkepov, S. Bulanov, J. Koga, M. Kando, K. Kondo, N. Rosanov, G. Korn, and S. Bulanov, Phys. Lett. A **379**, 2044 (2015).

[35] A. Gonoskov, A. Bashinov, I. Gonoskov, C. Harvey, A. Ilderton, A. Kim, M. Marklund, G. Mourou, and A. Sergeev, Phys. Rev. Lett. **113**, 014801 (2014).
[36] J. Schwinger, Phys. Rev. **82**, 664 (1951).
[37] A. M. Fedotov, N. B. Narozhny, G. Mourou, and G. Korn, Phys. Rev. Lett. **105**, 080402 (2010).
[38] *ELI Science and Technology with Ultra-Intense Lasers WHITE-BOOK*, edited by G. A. Mourou, G. Korn, W. Sandner, and J. L. Collier (Andreas Thoss, Berlin, 2011).
[39] L. W. Davis, Phys. Rev. A **19**, 1177 (1979).
[40] Y. I. Salamin and C. H. Keitel, Phys. Rev. Lett. **88**, 095005 (2002).
[41] T. Grismayer, M. Vranic, J. L. Martins, R. A. Fonseca, and L. O. Silva, Phys. Plasmas **23**, 056706 (2016).
[42] A. Fedotov, N. Narozhny, and A. Mironov, J. Phys.: Conf. Ser. **691**, 012023 (2016).
[43] M. Tamburini, A. Di Piazza, and C. H. Keitel, arXiv:1511.03987.
[44] A. Gruzinov, arXiv:1404.4615.